Available online at www.sciencedirect.com
SCIENCE DIRECT®

Journal of the European Ceramic Society 24 (2004) 3013–3020
www.elsevier.com/locate/jeurceramsoc

Laser crystallization studies of barium strontium titanate thin films

O. Baldus[a,*], R. Waser[b]

[a]Forschungszentrum Karlruhe GmbH, Institut für Materialforschung I, Postfach 3640, 76021 Karlsruhe, Germany
[b]Forschungszentrum Jülich, IFF and cni - center of nanoelectronic systems for information technology, 52425 Jülich, Germany

Received 24 September 2003; received in revised form 12 November 2003; accepted 21 November 2003

Abstract

It is reported about laser crystallization investigations of the amorphous thin-film ceramic $Ba_{0.7}Sr_{0.3}TiO_3$ (BST) with platinum electrodes on silicon substrates using ArF and KrF excimer lasers. The film thickness is an important parameter and was adjusted to minimize crack formation. For each film thickness the different laser parameters, such as pulse energy density, pulse number, and pulse length, were optimized. Thermal modeling was applied for the analysis of laser processing. During the preparation and crystallization process, the substrate temperature never exceeded 450 °C. For the first time, BST thin films have been crystallized by applying UV laser pulses for producing high k planar structures. The best electrical properties were obtained at a film thickness of 95 nm. The mechanisms resulting in the damaging of the thin films by short laser pulses were investigated systematically.

Keywords: Capacitors; Dielectric properties; Ferroelectric properties; Perovskite; Sintering; (Ba, Sr) TiO_3

1. Introduction

The work described here concentrates on the heating of amorphous ceramic thin films by nanosecond laser pulses in order to induce structural and electronic changes of their (electronic) properties in the heated region only.

The technological potential of electro ceramic thin films has been discussed in many publications.[1,2] A few drawbacks result from the conventional, quasi-stationary heat treatment of these new materials when integrating them in the circuit fabrication process. Consequently, two general reasons exist why laser processing is considered a useful tool for heat treatment in micro technology: The localized character of the heating is limited by the wavelength and the huge heating rates of up to 10^8 K/s for periods ranging from nanoseconds to milliseconds. This allows the precise control of thermally induced modifications in the zone under heat treatment only.

A large number (approx. 3500) of publications deal with laser annealing of ion-implanted or a:Si.[13,14] This technology often is part of new methods for the fabrication of thin-film transistors (approx. 200 patents in 2001). The main effects of laser crystallization are well-known and studied for semiconducting materials by qualitatively relating the major parameters, i.e. laser pulse wavelength, energy density, and duration, to the effects of crystallization and damaging.

For silicon (with the light penetration depth and thermo-physical properties differing from those of ceramics) the annealing effect with nanosecond pulses was found to very strongly depend on the energy density of the laser pulse. When the energy density is increased, the structure of the implanted layer is transformed consecutively from an amorphous to a polycrystalline phase, to a single crystal with a large number of twins and, finally, to a single crystal free of defects. The maximum permissible melting depth with respect to the electric properties of the laser-processed device gives the upper limit of the energy density. Surface roughness was smoothed and electric mobility of the silicon layers simultaneously increased with increasing pulse number.[3]

The number of publications concerning laser crystallization of ceramic thin films is much lower (approx. 15). The possibility of a phase transformation from an amorphous to an X-ray crystalline phase has been demonstrated.[4–7] Electrical data are missing in many cases, probably because of damages induced by laser processing. Processing parameters are either kinetic

* Corresponding author.
E-mail addresses: oliver.baldus@imf.fzk.de (O. Baldus), waser@iwe.rwth-aachen.de (R. Waser).

0955-2219/$ - see front matter © 2003 Elsevier Ltd. All rights reserved.
doi:10.1016/j.jeurceramsoc.2003.11.007

materials parameters like different optical and thermal properties or laser parameters like the pulse energy density that varies around an average of 100 mJ/cm^2.

The present paper predominantly presents experimental work on BST thin films. In a previous paper [4] it was reported that under certain conditions, damages are introduced in the BST thin film by irradiation with a KrF excimer laser. It shall be shown here that the film thickness is an important parameter which must be optimized to avoid damage from being produced during laser pulse treatment. The modeling of pulsed laser annealing together with a microscopic discussion of the laser sintering process will be the subjects of a next paper.

2. Experimental

2.1. Deposition of amorphous thin films

Thin films were prepared by a chemical solution deposition method from a stoichiometric ($Ba_{0.7}Sr_{0.3}$) Ti_1 solution.[8,9] The chemical solution deposition (CSD) technique offers the advantages of low costs, easy and exact variation of stoichiometry, and simple preparation routes. The BST precursor solutions are synthesized from alkaline earth propionate/titanium alkoxide solutions. The solution is diluted by the parent solvent (propionic acid). The chosen concentration of the solution is dependent on the required amorphous film thickness and amounts to 0.1M or 0.3M with respect to the A-site component (ABO_3 type). Deposition was performed by spin-on processing at a rate of 4000 rpm on a Pt-coated Si substrate. The platinum film was polycrystalline and 150 nm thick. The multilayer structure is shown in Fig. 3 on the left. Here, the BST film was additionally metallized for electrical characterization. The as-deposited coatings were pyrolized for 10 min at 450 °C on a hotplate. Thin films of 65, 95, 130, and 200 nm in thickness were produced. The films are X-ray amorphous. FTIR spectra reveal organic residues and carbonate compounds which cannot be disintegrated or eliminated completely below approx. 600 °C.[8]

Usually, a heat treatment of the amorphous as-deposited film at high temperatures (> 600 °C) is needed for crystallization. In this paper it is reported about the crystallization properties of ceramic thin films when the substrate temperature is kept constant at room temperature (25 °C).

2.2. Laser processing

Laser processing was carried out in ambient atmosphere at room temperature. The silicon wafer was positioned well on a clean metallic surface. Since the pulse diameter (~2 mm) was smaller than the sample (~10 mm), the sample was moved under the laser beam using a step motor-driven sample desk. For our experiments 1×1 cm^2 wafers were used. Two different excimer lasers were employed: Excimer lasers working with either ArF or KrF gas, resulting in excitation wavelengths of 193 nm and 248 nm, respectively. The pulse length was estimated using a gaussian fit of the pulse shape and then averaged, its values amounting to 16 ns (@193 nm) and 23 ns (@248 nm), respectively. The optical penetration depths of the two UV wavelengths applied were nearly the same (~20 nm). The average pulse diameter at a typical energy density of 100 mJ/cm^2 had a value of 2 mm. Due to these different pulse lengths, different laser crystallization results are expected with respect to the crystallization behavior and electrical properties of the thin films. The beam shaping system consisted of simple transmittive, focusing optical components specified for the particular wavelength.

The energy density was varied in the range of 10 mJ/cm^2 and 300 mJ/cm^2. The laser energy values were specified with a fault of 10%. The total number of pulses focused on one spot of the sample generally was in the range of 1 and 600.

2.3. Thin-film analysis

The thin films were characterized with respect to their degree of amorphicity and organic residues. The organic residues and carbonate compounds were identified using FTIR spectroscopy, whereas the level of amorphicity or crystallinity was determined qualitatively by X-ray diffraction. Further SEM and permittivity measurements generally were applied for the characterization of the laser-processed samples. A microscopic analysis technique (AFM, SNMS, TEM) is under development.

The thermal FEM model presented in the previous paper [4] has been improved by taking into account temperature-dependent variables, changing heat capacitance during melting, and an exact pulse modulation. The experimental results were interpreted based on the enhanced thermal FEM model.

3. Experimental results

Different processes like laser ablation, micro drilling, and many other materials processing methods modify the irradiated samples drastically, so that any damage is either of minor importance or acceptable. The laser annealing processes are used to transform the films in a well-defined manner by e.g. solid-solid phase transformations. Consequently, no damage of the film occurs. The possibility of crystallizing with ns-pulses has been demonstrated by several groups.[4,5] Unfortunately, the ceramic films often could not be characterized

electrically due to the occurrence of crack formation. To prevent damage of the planar structure, the ceramic film thickness was changed systematically.

3.1. 200 nm Thin films

At this film thickness, crack formation was evident at a laser pulse energy density of 50 mJ/cm^2 already.[4] As obvious from Fig. 1, this happened even at low pulse numbers and caused film ablation when the pulse number was increased.

Even for a small number of laser pulses applied (approx. 20), isolated cracks occurred. The damage threshold amounted to 40 mJ/cm^2 (@ 10 pulses). As a result, no undamaged crystalline films suitable for reliable capacitor test structures could be produced. The temperature [T(t,z)] in Fig. 2 suggests that only the upper part of the film is heated above the densification/crystallization temperature, whereas the lower part is kept far below 600 °C, such that high thermal stress gradients can be expected inside the BST film. It was shown [4] that substrate heating can essentially reduce crack formation at the expense of the localized character of heating.

3.2. 130 nm Thin films

The above-mentioned crack formation has not been observed when using thinner films. In contrast to thick films, the laser crystallization method with the KrF laser pulses (~23 ns) therefore seems to be well suited for thin films with a thickness of approx. 100 nm. Irradiation of 130 nm thick films with an energy density up to the damage threshold, which is approximately 260 mJ/cm^2 (@ 10 pulses) did not produce any cracks. At higher pulse numbers, additional effects influence this damage threshold, so that the maximum applicable energy density is reduced. This behavior shall be discussed in the qualitative interpretation below.

Fig. 3 (left) shows the SEM of a ceramic thin film processed with 100 mJ/cm^2 energy density, a pulse number of 500, and prepared as a plane capacitor with a sputtered top electrode. This film produces the highest permittivity ($\epsilon_r \sim 180$) with the lowest leakage current ($\tan\delta \sim 0.01$) as compared to equally thick films at variable energy densities. The film is very smooth (~1 nm RMS, measured by AFM). The morphology of the BST layer obviously is different at the top (white arrow in Fig. 3) and at the bottom (black arrow). Fig. 4 at the bottom shows the temperature calculated for a single 100 mJ/cm^2 KrF laser pulse during one heating cycle and the associated melting depth. The temperature slightly exceeds the melting temperature of BST at this laser energy. The melting depth amounts to ~9 nm. Fig. 4, top, illustrates the temperature profile near the surface of the wafer. The crystallization temperature of 600 °C [8] is exceeded in the entire film. At the same time, the temperature of the SiO_2 layer stays below 450 °C.

This allows three major conclusions to be drawn:

(1) The heat front—referring to 600 °C—seems to propagate through the entire film. The lower layer (black arrow) appears to grow on the polycrystalline platinum. Densification and crystallization reach the platinum layer. Possibly, this is the reason why no crack formation occurs for films thinner than 200 nm.
(2) The upper layer consists of molten-resolidified and probably partly crystallized material of approx. 9 nm thickness.
(3) The heating time of one pulse obviously is too short for a complete crystallization of the film, considering that 500 pulses were necessary for the crystallization.

The X-ray pattern in Fig. 5 at the top reveals that the crystallization processes are enhanced by an increased pulse energy density. As the X-ray beam has a larger diameter on the sample than the laser-crystallized part of the sample, an amorphous shoulder can be seen around 22°.

These laser-crystallized BST thin films could be characterized electrically after the deposition of a platinum top electrode (~0.1 mm^2, Fig. 5, bottom). A correlation was made between processing parameters and film

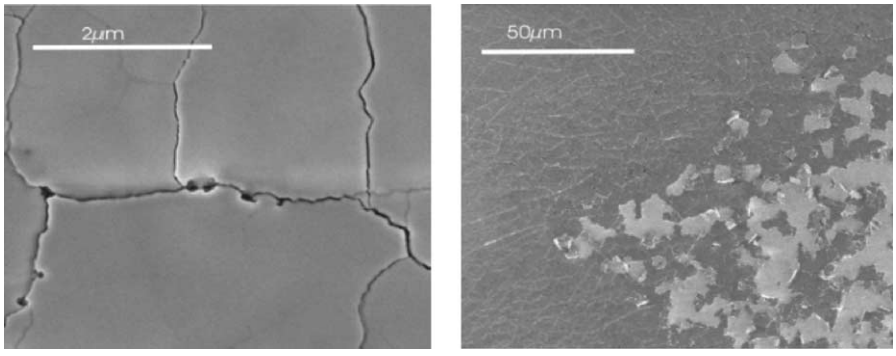

Fig. 1. SEM of 200 nm BST films processed with 50 mJ/cm^2 and 100 (left) and 500 (right) pulses. The ArF and KrF lasers induced cracks and, hence, damaging.

quality. The electrical characterization confirms the dependency of film quality (crystallinity) on the energy density. The lower threshold energy density for crystallization is approx. 50 mJ/cm^2 and the upper threshold for damaging @ 500 pulses is about 150 mJ/cm^2. The permittivity values for the thinner films shall be explained later.

The curves in Fig. 5 (bottom), have a maximum, which seems surprising. Higher laser energy densities lead to increased temperatures in the film, thus resulting in a faster crystallization. The maximum may be attributed to the melting depth being an important parameter: The amorphous state of the BST film after deposition and pyrolysis at 450 °C already seems to contain BST nuclei. This can be deduced from TEM and AFM analysis. When melting some part of the layer during laser processing, nucleation is suspended and restarted again under new nucleation and grain growth conditions. Concerning the melting depth (see Fig. 3, right), it is assumed that the molten and resolidified part is less crystalline than the heated non-molten part of the film, below which crystallization takes place step by step with many pulses. Consequently, the permittivity of the solidified part is smaller than the corresponding value of the non-molten part.

Compared to these results, the ArF laser-(pulse length ~16 ns)-processed films exhibited a similar behavior. Only at low pulse numbers (e.g. 20) did the ArF pulses produce non-crystalline films. When applying the KrF laser at a pulse length of ~23 ns, the ceramic films could be crystallized with 20 pulses only. This indicates that apart from the pulse number, also the pulse length is a deciding parameter. This can be explained well by using a continuum macroscopic crystallization model that is presently being developed.

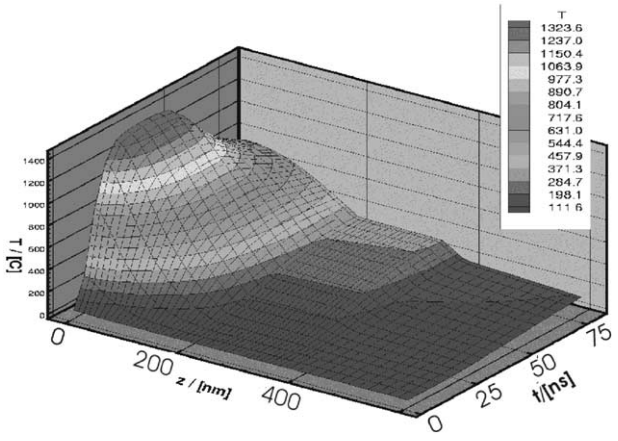

Fig. 2. The presented 3D model of temperature distribution after one KrF laser pulse of 80 mJ/cm^2 applied at the surface of the multilayer system shows that the part of the film close to the platinum is heated to temperatures far below 600 °C (light blue color).

3.3. 95 nm and 65 nm Thin films

Using thin films with a thickness of about 95 nm and 65 nm, crystallization can be achieved by applying the same UV laser pulses without the destructive stress cracks observed in the 200 nm layers. Laser pulse energy variations produced results similar to those reported for the 130 nm films. The laser pulses did not cause any damage up to approx. 300 mJ/cm^2 and 10 pulses (see Fig. 3, right, and 7). However, some differences can be noticed with respect to the pulse lengths when using the KrF and ArF lasers. Film morphology below the damage threshold is similar to that described above. In Fig. 3 on the right the resolidified (see black arrow) upper layer can be identified clearly. This sample shows the highest permittivity values of all ArF laser-processed thin films. The melting depth amounts to approx. 56 nm. Using the heat conduction model, the melting depth was calculated with the same material parameters as before. It is shown by the temperature profile in Fig. 4 at the bottom that the 95 nm BST thin film is heated far above 600 °C. Because of the high temperature profile obtained at 140 mJ/cm^2 despite the application of shorter ArF pulses, the heating period during one heating cycle is lengthened compared to the KrF pulse of 100 mJ/cm^2 for the 130 nm film. The profile decays on a longer time scale with temperatures above the melting point even though more than approx. 100 pulses were necessary to produce X-ray crystalline high-k films with this laser.

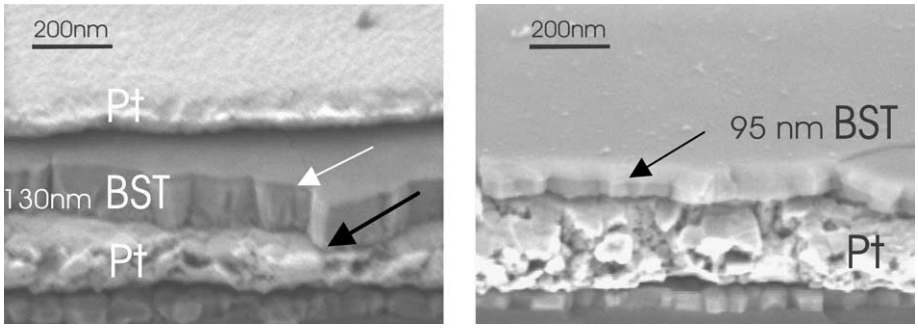

Fig 3. SEM cross sections of 130 nm (left) and 95 nm (right) thin films processed with the excimer laser. 100 mJ/cm^2 and 500 pulses (left), 50, 140, and 50 mJ/cm^2 in succession and 400 pulses (right).

The smooth, crack-free surface allows for further structuring to a capacitor. Experiments with pulse numbers smaller than 20 yielded crystalline films only with the longer KrF pulses, but resulted in bad electrical properties. Hence, there is also a correlation between the pulse number and the film quality. Below 100 pulses, crystalline peaks are not detected by XRD. The permittivity remains low and increases with a rising pulse number until the film cracks, similar to the representation given by Fig. 5 at the bottom. This result may be explained by a crystallization process that starts from already existing nuclei. Grains are growing in an amorphous surrounding, depending on time and temperature. Together with the thermal model, a Johnson–Mehl–Avrami model for physical modeling shall be presented to calculate this behavior as a function of the laser parameters.

The best results in this experimental series were achieved with a three-step process:

First, a cleaning step with low energy density, then a crystallization step of the part close to the substrate, and, finally, crystallization at low energy density of the resolidified part close to the surface.

The cleaning step comprises photolytic and pyrolytic ablation of contamination (e.g. C–H bonds) at the surface. This type of process [10,11] can be observed and identified by audio-visual signals due to the formation of plasma on the surface. The energy density of the pulses is smaller than 50 mJ/cm^2 and the process requires 5 pulses only. The crystallization step can be compared with the processes taking place in the 130 nm films (last section). In order to crystallize the molten and partly amorphous solidified part at the surface during the third step, the film is treated again at a lower energy density, such that the melting temperature will not be exceeded significantly (approx. 60 mJ/cm^2). Consequently, further grain growth at the surface can be induced.

Additionally, it was observed that the adhesive strength of the 65 nm films after the process is reduced relative to the laser power (see damage threshold in Fig. 9). This behavior results from the fact that the melting depth can no longer be neglected with respect to the film thickness. This is shown in Fig. 6, top, where the ceramic film is partly molten and, thus, destroyed. When the BST film is completely molten during laser processing, the liquid phase tends to form droplets on the platinum. Moreover, the influence of the platinum back electrode becomes more relevant to the formation of the temperature profile and the stress in the ceramic layer. For this reason, it was impossible to crystallize

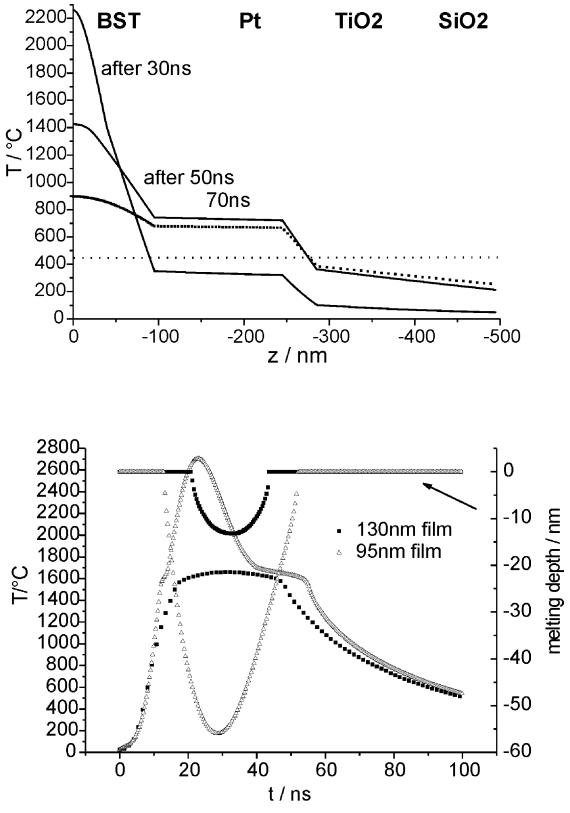

Fig. 4. Temperature calculations [T(z) top and T(t) below] for the samples shown in Fig. 3. The calculation of T(z) refers to the right sample in Fig. 3.

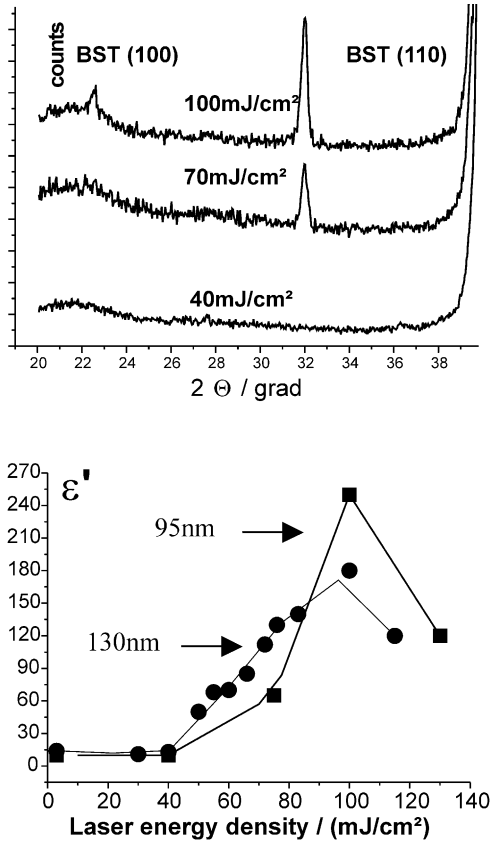

Fig. 5. X-ray pattern of the (100) and (110) diffraction peaks and permittivity ϵ' versus laser energy density @ 10k Hz for 130 nm (round) and 95 nm (square) films.

30 nm BST thin films with the excimer laser systems. In Fig. 7 a micrograph of the multilayer structure with a 65 nm BST thin film after the metallization with platinum is shown. The corresponding measurement of permittivity is displayed below. The highest relative permittivity values measured were smaller than those of the 95 nm films.

The temperature profiles calculated in Fig. 6 at the bottom reveal the influence of the film thickness on the laser sintering process. The substrate acts like a heat sink (particularly platinum and silicon) so that the 65 and 30 nm thin films cannot be heated above the melting temperature with this energy density (here 100 mJ/cm^2). This is shown by the thick lines in Fig. 6 at the bottom. Even though the temperature and, thus, the crystallization velocity can be increased by increasing the laser power, the interface temperature between the ceramic layer and the platinum layer has to be considered. A high platinum temperature generates thermal tension and above approximately 900 °C, delamination of the ceramic layer occurs due to a recrystallization process of the platinum. Therefore, the thinner films are destroyed before they can be heated as much as the thicker films. This is shown by the thinner lines in Fig. 6. Finally, the thermal load of the substrate shall be discussed using Fig. 4, top, as a basis. Since the maximum temperature at the bottom electrode is reached with a certain delay compared to the surface, calculated values are plotted after 30, 50, and 70 ns, respectively. The increase in temperature amounts to 400 °C at the maximum below the titanium oxide layer. This means that the goal of the development of a low-temperature process is achieved by reducing the temperature load of the substrate during the deposition and laser sintering of thin BST films.

4. Qualitative interpretation of crack formation

The chemical deposition method is not well suited for the complete elimination of the organic residues below a deposition temperature of 600 °C. These residues may contribute to crack formation during laser processing. A primary effect at a low energy density, above approx. 40 mJ/cm^2, is the densification of the ceramic thin film. To illustrate this result, an experiment with a beam diameter of approximately 100 μm is presented (Fig. 8). This sintering effect can be observed in nearly all experiments (at any film thickness) above a certain energy density (it can be identified by a color change of the film) and marks the lower threshold for the materials processing of these amorphous, dielectric CSD thin films. At such low pulse energies, no X-ray crystalline phase can be observed, even when 10 000 laser pulses

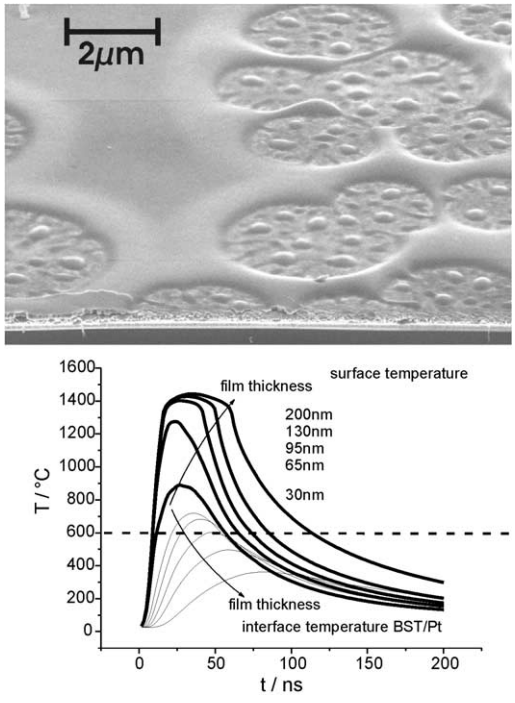

Fig. 6. SEM of a 65 nm BST thin film (cross section), 270 mJ/cm^2 with the ArF laser, 300 pulses, bottom: Temperature profiles calculated for a single 100 mJ/cm^2 KrF pulse at varying film thicknesses (from 30 to 200 nm). Thick lines—surface temperature, thin lines—interface temperature between the BST and Pt layer.

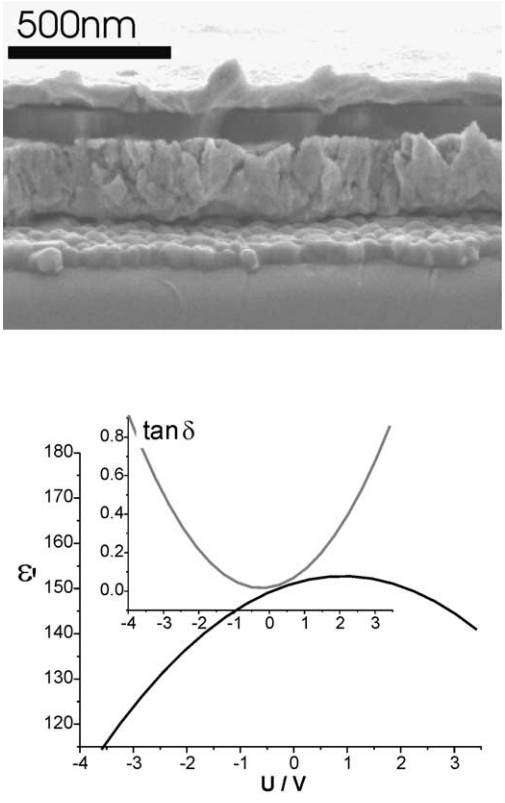

Fig. 7. SEM of a 65 nm BST thin film (cross section), successive application of 50, 110, and 70 mJ/cm^2 @ 30, 300, and 30 pulses and permittivity measured for this 65 nm BST film.

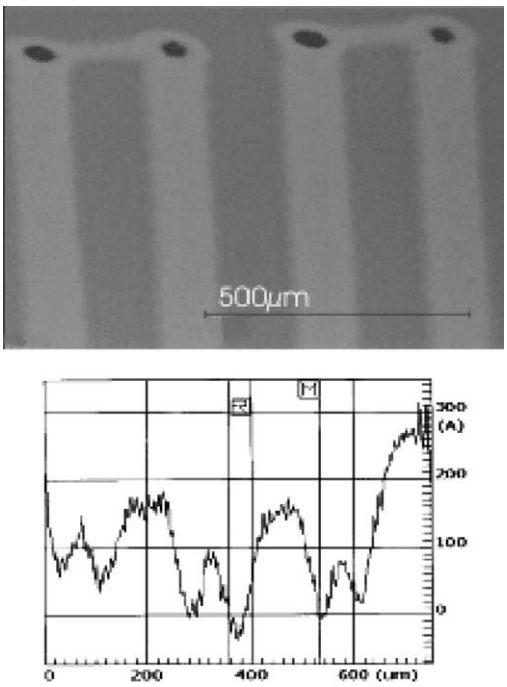

Fig. 8. Microscope and profilometer image of laser tracks on a ceramic sample. The densified material appears brighter.

are applied. The cracks in the 200 nm films at the same energy density are therefore supposed to be caused by stress due to inhomogeneous heating and densification and by residual stress of the as-deposited film. A two-layer system is formed by inhomogeneous crystallization of crystallized (condensed) combined with amorphous (non-condensed) material. Apart from vertical inhomogeneities, also plane inhomogeneities exist in the film due to the small pulse diameter. Thus, a crystalline lens is formed in the layer and the tensile stress is expected to grow strongly with gradual sintering. Additional compressive stress arises from the inhibited thermal expansion during heating, followed by tensile stress due to densification and crystallization following temperature homogenization.

The 130 and 95 nm films were found to be resistant to thermal shocks. After a reproducible pulse number, damaging occurs, followed by ablation. This is probably due to small cracks that prevent heat conduction in some directions and lead to overheating and melting. With rising energy density, the maximum melting depth is reached when the film is completely molten and droplets are formed. Even a nearly completely molten film is unstable already. The damage threshold in the experiment with ten laser pulses is obvious from Fig. 9. The tolerance of the given values primarily results from the variation of the pulse energy of the laser systems rather than from the film properties.

Other reasons for damaging are a strong contamination of the surface, which has the effect of a thin additional layer [11,12] and rough particles that promote the

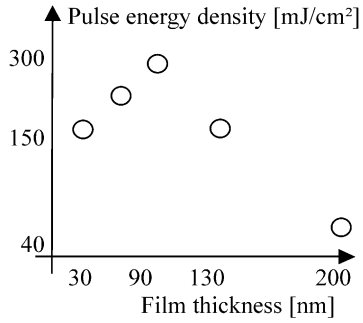

Fig. 9. Experimentally acquired damage thresholds (with approximately 10 pulses each) at variable film thickness.

formation of droplets. In a previous paper [4] the decomposition of organic residues during the laser processing was presented following deposition at a temperature of 250 °C only. It takes places simultaneously with nucleation and grain growth.

5. Conclusions

A well-defined laser pulse energy and pulse number result in a film thickness of BST films deposited by chemical solution deposition, which is suitable for laser crystallization without damaging. It is assumed that the sintering effect during pulsed laser heating produces cracks in thick films. In this case, the melting depth is of no importance to laser processing. Melting depth must not exceed the film thickness to avoid damaging in thinner films. The thinner the film thickness, the smaller is the maximum applicable pulse energy in films of less than 100 nm. More than approx. 100 pulses are needed for the formation of the perovskite phase in the solid amorphous CSD film when applying 16 ns ArF pulses. Using KrF laser pulses of 23 ns pulse length, crystallization is possible with slightly lower pulse numbers and energy densities and, hence, with a smaller melting depth. The thickness of the underlying platinum layer (here 150 nm) should probably be reduced for thinner films (<60 nm) in order to decrease the contact temperature at the bottom electrode.

A low-temperature process for producing reliable planar BST thin-film capacitors with laser crystallization has been reported. Since no post-annealing was performed after sputtering the top platinum contacts, the electrical properties are competitive with those of traditional BST films crystallized by furnace annealing. Examinations of laser-treated amorphous films without organic residues are in preparation.

Acknowledgements

This work was performed at the Jülich research center. The opportunity to use the laser equipment of

the Institut für Lasertechnik (ILT) in Aachen is acknowledged.

References

1. Koteckik, D. E., *IBM J. Res. Develop*. 1999, **43**(3), 5.
2. Isaak, R. D., *IBM J. Res. Develop*. 2000, **44**(3), 5.
3. Brotherton, S. D., Ayres, J. R. and Trainor, M., *Thin Solid Films*, 1999, **337**, 188–195.
4. Baldus, O. and Waser, R., *Integrated Ferroelectrics*, 2000, **30**, 129–138.
5. Lu, X. M. and Wang, Y. N. *Appl. Phys. Lett*. 1995, **66**(19), 5.
6. Kwang Soo Seol and Choi, H. I., *J. Mater. Res*. 2001, **16**(7), 7.
7. Donohue, P., Brown, A.R. and Watton, A., *Proceedings of SPIE* 2000, **4130**.
8. Hoffmann, S. and Waser, R., *Mat. Res. Soc. Symp. Proc*. 1997, **474**.
9. Hasenkox, U. and Waser, R., *J. Sol-Gel Science a. Techn*, 1998, **12**, 67–79.
10. Cain, S., Burns, F. C. and Otis, C. E. *J. Appl. Phys*. 1992; **71**(9).
11. Stauter, C., Fontaine, J., Engel, Th., Biernaux, A. Conference Title: Proceedings of Laser *Processing: Surface Treatment and Film Deposition* (ISBN 0 7923 3901 0), 1996, pp: 881.
12. Lu, Y. F., Song, W. D., Hong, M. H., Ren, Z. and Zheng, Y. W., *Proceedings of the SPIE*, 2000, **371**, 4088.
13. Stamm, U., Patzel, R., Bragin, I. and Basting, D. *Proc. SPIE-Int. Soc.Opt. Eng*., 1997, **3092**, 485–92.
14. Gotz, G., Andra, W. and Wagner, M. *Proc. of the Fourth Int. Conf., Ion Implantation*. 504, Springer-Nr. 3 540 12491 8, 1983.